

An Experimental and Analytical Investigation of Rectangular Synthetic Jets

Gopi Krishnan

Kamran Mohseni¹

e-mail: mohseni@colorado.edu

Department of Aerospace Sciences,
University of Colorado,
Boulder, CO 80309-429

In this paper the flow field of a rectangular synthetic jet driven by a piezoelectric membrane issuing into a quiescent environment is studied. The similarities exhibited by synthetic and continuous turbulent jets lead to the hypothesis that a rectangular synthetic jet within a limited region downstream of the orifice be modeled using similarity analysis just as a continuous planar jet. Accordingly, the jet is modeled using the classic two-dimensional solution to a continuous jet, where the virtual viscosity coefficient of the continuous turbulent jet is replaced with that measured for a synthetic jet. The virtual viscosity of the synthetic jet at a particular axial location is related to the spreading rate and velocity decay rate of the jet. Hot-wire anemometry is used to characterize the flow downstream of the orifice. The flow field of rectangular synthetic jets is thought to consist of four regions as distinguished by the centerline velocity decay. The regions are the developing, the quasi-two-dimensional, the transitional, and the axisymmetric regions. It is in the quasi-two-dimensional region that the planar model applies, and where indeed the jet exhibits self-similar behavior as distinguished by the collapse of the lateral time average velocity profiles when scaled. Furthermore, within this region the spanwise velocity profiles display a saddleback profile that is attributed to the secondary flow generated at the smaller edges of the rectangular orifice. The scaled spreading and decay rates are seen to increase with stroke ratio and be independent of Reynolds number. However, the geometry of the actuator is seen to additionally affect the external characteristics of the jet. The eddy viscosities of the synthetic jets under consideration are shown to be larger than equivalent continuous turbulent jets. This enhanced eddy viscosity is attributed to the additional mixing brought about by the introduction of the periodic vortical structures in synthetic jets and their ensuing break down and transition to turbulence. Further, a semi-empirical modeling approach is proposed, the final objective of which is to obtain a functional relationship between the parameters that describe the external flow field of the synthetic jet and the input operational parameters to the system.

[DOI: 10.1115/1.4000422]

1 Introduction

A synthetic jet is a type of pulsatile jet that results from the formation and interaction of vortex rings or pairs [1]. A common method of generating a synthetic jet employs a cavity-diaphragm setup and is the method used in this experiment. The setup consists of a sealed cavity with a flexible vibrating diaphragm on one end and an orifice on the other. As shown in Fig. 1, the synthesis is comprised of a cycle with two strokes, suction, and ejection. During the suction stroke the diaphragm moves away from the orifice increasing the volume of the cavity and subsequently decreasing the pressure within, resulting in the entrainment of low momentum fluid into the cavity. During the ejection stroke the diaphragm moves toward the orifice, resulting in the expulsion of fluid through the orifice. If a formation criteria is met [2,3], the shear layer formed at the edge of the orifice rolls up to form a vortical structure that travels downstream due to its self-induced velocity. A series of such suction-ejection strokes results in the formation of a train of vortical structures moving away from the orifice. These coherent structures may then form a laminar jet, or interact and break down in a transition toward a turbulent jet that is directed downstream.

This operational principle allows for the synthetic jet to be syn-

thesized entirely from the surrounding medium. This implies a zero net mass flux across the actuator boundary. However, on account of the asymmetry of the system a net momentum flux is imparted to the external flow. The lack of plumbing provides added benefits of reduced size, weight, and fabrication complexity. Additionally, the periodic vortical structures introduced into the flow exhibit an ability to influence the environment at a variety of length scales. All these properties make synthetic jets attractive in a number of applications that include active flow control [4–6], electronics cooling [7,8], fluid mixing [9], as well as both aerial [10–13] and underwater propulsion [14,15].

Synthetic jet actuators occur primarily in axisymmetric [16–18] and rectangular [19–21] configurations, where the latter is studied in this paper. Rectangular synthetic jets differ from circular ones in terms of the vortex dynamics involved in the evolution of the jet and the time average and fluctuating velocity characteristics in the far field [22,23]. The primary mechanism accountable for jet entrainment in the near field of continuous circular jets is known to be vortex ring formation and merging. In continuous rectangular jets an additional mode of axis switching of the vortical structures is understood to enhance entrainment. Synthetic rectangular jets have been shown to engage in behavior similar to continuous rectangular jets in terms of the complex evolution that the coherent vortical structures undergo as they switch axis, interact, and break down [24,25]. At the same time it is known that the primary mechanism for the generation of large-scale coherent structures is different in both continuous and synthetic jets.

A schematic of a rectangular synthetic jet is shown in Fig. 2. A single rectangular shaped vortical structure is shown in the near

¹Corresponding author.

Contributed by the Fluids Engineering Division of ASME for publication in the JOURNAL OF FLUIDS ENGINEERING. Manuscript received November 29, 2008; final manuscript received September 25, 2009; published online November 10, 2009. Editor: Joseph Katz.

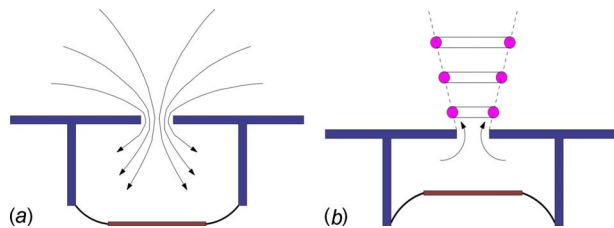


Fig. 1 Schematic of synthetic jet operation

field, while the time average velocity profiles are shown in far field. The x , y , and z coordinates may hereafter be referred to as the streamwise, transverse, and spanwise directions as well. During the expulsion stroke the shear layer formed at the orifice rolls up to form a rectangular shaped vortical structure, in contrast to the counter-rotating roller vortices present in an idealized two-dimensional jet. The differential, self-induced velocity on account of the variation in curvature along the vortical structure results in the section of the vortex structure parallel to the major axis, moving faster than that along the minor axis causing the structure to deform [8]. As the vortex structure moves downstream, the continued self-induced deformation under certain conditions leads to axis switching, reconnection, and bifurcation [25,26]. Simultaneously, azimuthal instabilities start to develop and add further complexity to structures topology [19,25,27]. The interactions between such successively deformed coherent structures results in the formation of braid or rib vortices. This in turn induces further deformation and elicits instabilities leading to the breakdown of the vortical structures. Due to the unstable large-scale coherent structures and the enhanced small-scale mixing, rectangular nozzles serve as a passive method of enhancing mixing in a synthetic jet. This rapid breakdown results in rectangular synthetic jets exhibiting a quicker transition to turbulence and increased entrainment in comparison with round synthetic jets [26].

The far field of synthetic and continuous jets exhibit similarities as well. The transverse time average and fluctuating velocity profiles in synthetic jets exhibit self-similarity as distinguished by the collapse of the profiles when normalized by appropriate variables [19]. At low Reynolds numbers, synthetic jets show some deviation from planar continuous jets in terms of the centerline velocity decay not exhibiting $x^{-1/2}$ behavior, and the jet width not showing linear growth. This deviation was attributed to the presence of a pressure gradient formed due to the periodic suction strokes [8,19]. However, at higher Reynolds numbers synthetic jets exhibit both decay and spreading behavior characteristic of planar continuous jets [20]. Thus suggesting that perhaps there is some threshold value to Reynolds number at a given Strouhal number. The synthetic jets do however develop more quickly, with both the centerline velocity decay and jet spread increasing more rapidly than equivalent planar turbulent continuous jets.

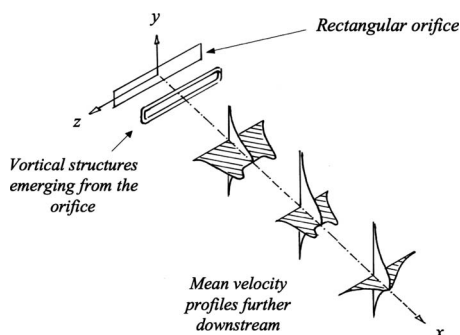


Fig. 2 Schematic of the evolution of a rectangular synthetic jet

It should be noted however that the exact nature of the evolution of both the near and far field of the synthetic jet are sensitive to initial conditions that include nozzle geometry [8] and actuator parameters. Two nondimensional variables, namely, the stroke ratio and Reynolds number have been identified as the primary factors that influence synthetic jets [19]. The stroke ratio is representative of a length of the slug of fluid ejected from the orifice during the ejection stroke. The Reynolds number embodies the velocity of this ejected slug. The explicit definitions are given later in the paper.

In order to design rectangular synthetic jets for various applications, a model of the evolution of the external jet at least in the time average sense is required. The external flow field of rectangular synthetic jets may be modeled using either numerical [21,24,25,28–30] or semi-analytical [19–21] techniques, where each has its own advantages and disadvantages. The numerical approach provides detailed information of the flow at the expense of computational time. The semi-analytical methods on the other hand are simpler but require experimental investment to extract empirical parameters. This paper builds upon the latter semi-analytical method to suggest a modeling approach that circumvents the computational cost of a detailed numerical analysis, while at the same time captures the essential physics required for further optimization studies.

The semi-analytical approach is built upon the previously mentioned facts that the far fields of synthetic jets resemble that of turbulent continuous jets in their self-similarity, with the synthetic jet spreading and decaying more rapidly [19,20]. This then suggests that the turbulent planar jet model may be extended to a synthetic jet by taking into account the increased spreading rate through an enhanced turbulent mixing coefficient associated with the synthetic jet. The previous semi-analytical descriptions of the external flow field employed velocity profiles identical to that of planar turbulent jets to just fit the synthetic jet velocity profiles. The present work goes further in suggesting that the external flow field of the synthetic jet may be characterized and systematically modeled based on the classical planar jet derivation. Additionally, the differences in the far field between synthetic and continuous jets are ascribed to an eddy viscosity coefficient that encompasses the magnitude of momentum transfer in the flow. This study is the first step in developing and obtaining a functional, semi-empirical relationship between the characteristics of the external jet and the critical input parameters of the actuator. The framework may be used in the future as a universal guideline for designing synthetic jet actuators during a first design iteration.

This paper is outlined as follows. Section 2 lays out the theoretical models of the external flow field of the synthetic jet, followed by a model of the actuator. The experimental setup for the measurement of the velocity field and diaphragm deflection is then described in Sec. 3. After which the results are presented and discussed in Sec. 4. In Sec. 5, the conclusions and future work are summarized.

2 Theoretical Modeling

A complete model for a rectangular synthetic jet must detail the relationship between the input driving parameters and geometry of the actuator, to the external characteristics of the ensuing jet. In this paper, the geometry of the actuator is not studied and is the topic of future work addressed in Sec. 5. With this said, in using a piezoelectrically driven actuator the driving parameters are frequency (f) and Voltage (V_d) in the case of a sinusoidal driving function. This input translates to a deflection of the membrane that depends on the system dynamics of the actuator cavity and diaphragm. This deflection and frequency may then be expressed as nondimensional actuator related parameters ($L/h, Re_{U_0}$). The actuator parameters subsequently influence the far field of the issuing synthetic jet that may be characterized by a decay rate (K_d) and spreading rate (K_b). This framework relating the identified input variables to the output variables is the basis of the semi-

analytical modeling approach mentioned in Sec. 1. In Sec. 2.1 a model for the external flow field in terms of velocity profiles, spreading rates, and decay rates are outlined first. Following which a model relating the amplitude of deflection and frequency of the driving diaphragm to the nondimensional actuator parameters is presented.

2.1 Time Average Flow Field. Consider the region of the synthetic jet flow where the periodically formed vortical structures cease to be coherent and a turbulent jet directed downstream exists (Fig. 2). In this regime, the influence of the edge has not completely permeated the flow and the transverse velocity profiles may be thought to be independent of the spanwise coordinate. The jet may be viewed to issue from a long, narrow slot (momentum source) into the external quiescent environment where it may be admissible to describe the time average velocities in the jet by boundary layer equations. The basic premise in this section is that the observed far field properties of a synthetic jet allow one to follow the classic modeling approach for turbulent continuous jets [31], with the key addition being the replacement of the eddy viscosity of the continuous turbulent jet with that of the synthetic jet. Following the classic derivation of the jet [31], the boundary layer equations with no pressure gradient may be expressed as

$$u \frac{\partial u}{\partial x} + v \frac{\partial u}{\partial y} = \frac{1}{\rho} \frac{\partial \tau}{\partial y}, \quad \text{and} \quad \frac{\partial u}{\partial x} + \frac{\partial v}{\partial y} = 0 \quad (1)$$

where τ is the turbulent shear stress and ρ is the fluid density. The turbulent shear stress may be related to the time average velocity by an eddy viscosity approximation given as $\tau = \rho \varepsilon \frac{\partial u}{\partial y}$, where ε is a coefficient of eddy viscosity or virtual viscosity. The eddy viscosity hypothesis assumes that the momentum transfer in a turbulent flow is due to eddies in turbulence, in contrast to laminar flow where molecular diffusion is responsible for momentum transport. With the eddy viscosity characterizing the time average momentum transfer due to turbulent fluctuations, previous observations of the enhanced spreading rate immediately suggest that a synthetic jet has a higher eddy viscosity than a continuous jet. Then based on the similarity between synthetic rectangular and continuous jets, and the enhanced spreading rates of the former over the latter, it is hypothesized here that synthetic jets may be modeled as continuous planar jets with the replacement of the eddy viscosity of the continuous turbulent jet with the enhanced value associated with a synthetic jet.

Assuming that the evolution of the jet is dependent only on local length and velocity scales, and lacks memory of the slot dimensions itself, the streamwise time average velocity profiles may be considered self-similar. From the mixing length hypothesis and conservation of streamwise momentum it may be shown that the characteristic length and velocity of the jet scale as $b \propto x$ and $u \propto x^{1/2}$, respectively. The self-similar assumption then leads to a streamwise velocity profile of the form $u = x^{1/2} g(y/x)$. The similarity variable is written as $\eta = \sigma y/x$, where σ is a free constant. As a consequence of the form of self-similarity assumed, the eddy viscosity is proportional to the distance downstream of the momentum source and centerline velocity, $\varepsilon \propto x u_c$. This assumption implies that the eddy viscosity varies only in the streamwise direction and is constant in the lateral direction.

The governing equations along with the self-similar velocity profile assumption, the eddy viscosity model, and boundary conditions result in the reduction in the boundary layer equations to an ordinary differential equation, $\varphi^2 + \varphi' = 1$. This is the same equation obtained for a two-dimensional laminar jet where $\varphi = \tanh(\eta)$ is a solution. From the conservation of momentum and the assumed form of the velocity distribution, the solutions for the velocity components are then written as

$$u = \frac{\sqrt{3}}{2} \sqrt{\frac{K\sigma}{x}} (1 - \tanh^2 \eta), \quad \text{and} \quad (2)$$

$$v = \frac{\sqrt{3}}{4} \sqrt{\frac{K}{x\sigma}} (2\eta(1 - \tanh^2 \eta) - \tanh \eta)$$

where K is the kinematic momentum per unit length and is a measure of the strength of the jet, and may be obtained from $\rho K = J = \rho \int_{-\infty}^{+\infty} u^2 dy$. It is important to note here that the above analysis assumes a constant momentum flux in the streamwise direction. While this is readily applicable to continuous jets, in synthetic jets it has been reported that the momentum flux at the orifice is higher than that in the far field [19,21]. The momentum flux was shown to decrease in the near field of the jet due to an adverse pressure gradient, and then asymptote in the far field to some fraction of the exit momentum flux. It is this reduced asymptotic value of the momentum flux that should serve as the magnitude of the driving momentum flux in the above similarity analysis for the synthetic jet, and not the exit momentum flux at the orifice of the actuator. However if it is assumed that the asymptotic value applies to all synthetic jets equally, then the use of the exit momentum flux as a scale is permissible, with the added benefit that it may be obtained from an actuator model.

The centerline streamwise velocity may be expressed as

$$U_c = \frac{\sqrt{3}}{2} \sqrt{\frac{K\sigma}{x}} = S_u \frac{1}{\sqrt{x}} \quad (3)$$

where S_u is the centerline velocity jet decay rate. In scaling this equation, the centerline velocity decay may be expressed as

$$\left(\frac{U_o}{U_c}\right)^2 = K_u \left(\frac{x - x_{o,u}}{h}\right) \quad (4)$$

where U_o is an average velocity associated with the actuator, h is the width of the rectangular slot, K_u is a scaled decay rate of the jet, and $x_{o,u}$ is the axial location of the virtual origin based on the centerline velocity. The location of the virtual origin is obtained from the intersection of the line asymptote of $1/U_c$ and the abscissa (x), and may be thought of as the self-similarity origin of the jet.

The width of the jet at a particular axial station may be characterized by a half width $b_{1/2}$ defined as the lateral distance from the centerline at which the streamwise velocity drops to half the centerline velocity. The axial variation in the jet width may be expressed either as $b_{1/2} = S_b x$ or identically as

$$\frac{b_{1/2}}{h} = K_b \left(\frac{x - x_{o,b}}{h}\right) \quad (5)$$

where S_b and K_b are the spreading rates, and $x_{o,b}$ is the axial location of the virtual origin based on the jet width. From Eqs. (2)–(4) the free constant σ in the similarity variable is related to the spreading rate as $\sigma \approx 0.88/S_b$. From Prandtl's second hypothesis for eddy viscosity [32], the eddy viscosity may be expressed as

$$\varepsilon \approx \frac{0.28 U_c b_{1/2}}{\sigma} \approx 0.32 S_u S_b^2 \sqrt{x} \approx \frac{0.32 U_o \sqrt{hx} K_b^2}{\sqrt{K_u}} \quad (6)$$

From Eq. (6) it is seen that the eddy viscosity (i) varies in the axial direction as \sqrt{x} , (ii) depends on both the dimensions of the orifice and the exit velocity of the jet, and (iii) increases with the square of the spreading rate.

In summary, Eqs. (2), (4), and (5) describe the velocity profiles, jet decay, and spreading rate, and are used to characterize the external flow field of the synthetic jet. The inputs required are U_o, h, K_u, K_b . The averaged exit velocity is obtained from an incompressible model described in Sec. 2.2, the orifice width is

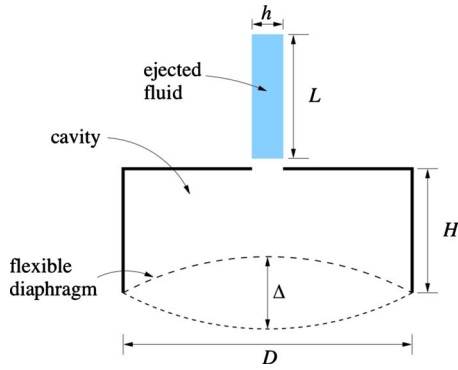


Fig. 3 Schematic of an incompressible actuator model, where the volume of fluid displaced by the diaphragm is ejected through the orifice in the form of a slug

know beforehand, while the decay and spreading rates are obtained from measurements of the external flow field described in Sec. 3.

2.2 Actuator Model. In a quiescent environment the evolution of a synthetic jet depends on several parameters that include (i) the actuator geometry, (ii) the properties of the working fluid, and (iii) the actuation parameters. Ignoring the explicit nondimensional geometric parameters, two nondimensional actuation-related variables have been proposed and established as key parameters governing the evolution and development of synthetic jets [19]. They are the stroke ratio (L/h) and Reynolds number (Re_{U_o}) based on the ejection cycle.

It has been shown that the flow in the actuator may be considered incompressible if the frequency of actuation is far less than the Helmholtz frequency [33]. This will later be shown to be the case which permits the use of an incompressible model to estimate the exit jet velocities. Figure 3 shows a schematic representation of the model, where it is assumed that the volume displaced by the membrane is equal to the volume ejected from the orifice. The length of the slot (w) is not shown in the figure. The stroke ratio is defined as the ratio of the stroke length (L) to the orifice width (h), where the stroke length may be thought of as the length of a hypothetical slug of fluid that is ejected from the orifice during the expulsion stroke [34].

To obtain the volume displaced by the membrane, the shape of the deflected membrane and the central amplitude are required. It is assumed that the shape of the membrane may be modeled as the static deflection of the circular membrane clamped at the edges subject to a uniform load. The deflection profile yields [35]

$$\delta(r) = \frac{\Delta}{2} \left[1 - \frac{r^2}{R^2} + \frac{2r^2}{R^2} \ln\left(\frac{r}{R}\right) \right] \quad (7)$$

where r is the radial coordinate and R is the radius of the membrane. The total volume displaced by the membrane during the expulsion stroke from the trough to the crest is $Q = 2 \int_0^R \delta(r) 2\pi r dr$, and is equal to 0.25 for the deflection profile considered.

With the ejected volume approximated as a rectangular slug of fluid with the same cross section as the exit orifice ($w \times h$) and equating the volume of the displaced fluid to that of the slug, the stroke ratio is determined to be

$$\frac{L}{h} = \frac{0.25 \pi D^2 \Delta}{4wh^2} \quad (8)$$

The periodic nature of synthetic jets allows for the velocity scales to be defined based on either volume or momentum flux [36]. If based on volume flux the velocity scale is given as $U_o = L/T = fL$, and if based on momentum flux it is given as U_o

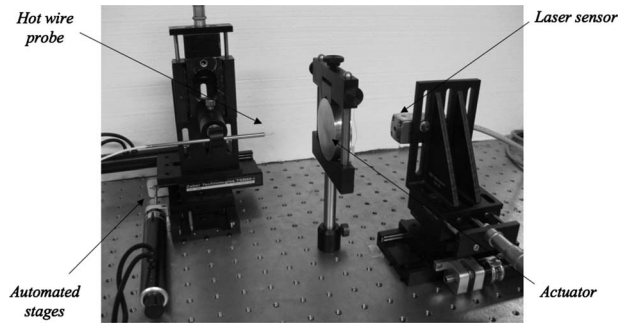


Fig. 4 Experimental setup

$= \sqrt{2}L/T = \sqrt{2}fL$. It is more appropriate to use the velocity scale based on momentum flux here, as the self-similar jet solutions employed in this study define equivalent jets based on the same momentum flux and not mass flux. Consequently, the Reynolds number is defined as

$$Re_{U_o} = \frac{\sqrt{2}Lfh}{\nu} \quad (9)$$

The Reynolds number is explicitly seen to vary with both membrane driving frequency and amplitude, with the stroke ratio appearing to be independent of frequency. This independence of stroke ratio on frequency is not entirely accurate as the use of a piezoelectric diaphragm as a driver gives rise to the coupling between frequency and deflection, and consequently stroke ratio. However, for purposes of calculating the jet parameters the model is seen to serve the purpose. Equations (8) and (9) now relate the input driving deflection amplitude (Δ) and frequency (f) to the nondimensional actuator parameters ($L/h, Re_{U_o}$).

In summary, Secs. 2.1 and 2.2 yield the following methodology that may be used in modeling synthetic jets. (i) Given a known input driving frequency (f) and voltage (V_d) the centerline deflection (Δ) is either determined from a model of the system [33] or measured experimentally (as was done in this study). (ii) The actuator parameters ($L/h, Re_{U_o}$) are calculated from Eqs. (8) and (9). (iii) The spreading rate (K_b) and velocity decay rate (K_u) are experimentally determined from the flow field. (iv) The eddy viscosity is calculated from Eq. (6). (v) The analytical velocity profiles are then modeled using Eq. (2). (vi) Steps (i) through (v) are repeated for the same actuator at different operating conditions so that a relationship between the actuator parameters output (K_b, K_u) and actuator parameters ($L/h, Re_{U_o}$) may be determined.

It is apparent that the above methodology is appropriate for a single actuator. A more universal model requires a design of experiments that may isolate the effect of individual geometric parameters of the output. In this paper, steps (i)–(vi) are carried out over a limited input range. Next, the experimental setup used to determine the parameters are described.

3 Experimental Setup

From Sec. 2 the inputs to the model include (i) the spreading rate of the jet (K_b), (ii) the centerline velocity decay of the jet (K_u), (iii) the central deflection of the membrane (Δ), and (iv) the frequency of oscillation (f). In this section the experimental setup to measure the parameters are described.

3.1 External Flow Field. The experimental setup to measure the external flow field is shown in Fig. 4 and consisted of a synthetic jet actuator, computer controlled stages, and a hot-wire probe, all of which are placed in a large Plexiglas enclosure to isolate the jet from external disturbances. To evaluate the effect of the size of the Plexiglas enclosure on the flow field, initial experiments were conducted with the setup placed in a small box (1



Fig. 5 Actuator with a rectangular slot orifice along side a dime provided for scale

$\times 0.5 \times 0.5 \text{ m}^3$) and a large box ($1.5 \times 1 \times 1 \text{ m}^3$). The results were then compared with the setup located in the ambient laboratory environment, with the doors closed and ventilation systems turned off. With the jets operating for 5 min in the enclosure to establish a stationary flow state, no significant differences were observed in the time average and rms velocity profiles. Thus, the smallest enclosure was used to isolate the jet flow field from the ambient conditions.

The actuator used was a piezoelectrically driven apparatus that consists of a circular piezomembrane and an aluminum housing. The piezoelectric element was sandwiched between the two circular aluminum elements, which when screwed together form a cavity with a rectangular orifice on one end and a flexible membrane on the other (Fig. 5). The piezo element was connected to a power amplifier (fixed gain of $10\times$) driven by a sinusoidal signal from a function generator. Two actuators were tested for this study. The dimensions common to both included nozzle length $w = 38.6 \text{ mm}$, nozzle depth $t = 0.5 \text{ mm}$, cavity diameter $D = 44.5 \text{ mm}$, and cavity height $H = 2 \text{ mm}$, with the difference being the slot width $h = 0.5 \text{ mm}$ and 0.85 mm . This translated to aspect ratios (w/h) of 77:1 (Actuator 1) and 45:1 (Actuator 2). It was observed that at aspect ratios less than 20:1, a jet with a measurable quasiplanar region was not present and hence not considered in this study.

The velocity measurements were made using a single normal hotwire probe operating in constant temperature anemometry (CTA) mode. The probe wire was 1.25 mm long and $5 \mu\text{m}$ in diameter and aligned such that the prongs were parallel to the streamwise axis or the plane jet. The signal obtained at a sampling rate of 50 kHz was fed through a low pass filter with a cutoff frequency of 10 kHz . The hot-wire was calibrated in an iterative procedure [37] with a fourth order polynomial curve used to convert voltage to velocity. The uncertainty in the time average velocity measurements were estimated to be $\pm 2\%$ for velocities greater than 1.75 m/s and $\pm 10\%$ for velocities less at 0.75 m/s , with the largest contribution to the uncertainty arising from the calibration process. It should be noted that quantifying the uncertainty associated with single hot-wire measurements in regions where the fluid velocity is both low and contains a significant radial component was not assessed.

It should be noted that the issues arising from the use of single hot-wire probes is that associated with directional ambiguity and measurements of very low velocities. While oscillatory flow and low velocities are encountered in the near field and outer edges of the flow, respectively, neither are expected to adversely change the conclusions drawn in the study as the purpose of the experiment is

not so much as quantify the velocity components themselves but to verify a modeling method and qualitatively evaluate the effect of actuator parameters on the jet parameters.

The hot-wire probe was affixed to a holder positioned on two computer controlled stages capable of traversing the horizontal plane. In order to characterize the flow field the probe was moved in the horizontal plane of the orifice in discrete intervals, where at each location the flow was sampled for 5 s. The extent over which the measurements were made was dependent on the actuator. For actuator 1, the centerline velocity measurements were made at axial locations ranging from $6x/h$ to $65x/h$. Upon identifying the quasi-two-dimensional region, velocity profiles were obtained at axial positions ranging from $12x/h$ to $32x/h$ in intervals of $4x/h$. The spanwise and lateral extent of measurements about the central axis of the jet were $\pm 45z/h$ and $\pm 12y/h$. The velocity profile, half width of the jet, centerline velocity, and the location of virtual origin were then obtained from the flow measurements. K_u and K_b were subsequently calculated based on these data.

3.2 Diaphragm Deflection. The setup to measure the centerline deflection of the piezoelectric membrane consisted of a laser nanosensor, a movable stage, and a small sliver of silicon (not shown) affixed to the center of the piezoelectric membrane while it was housed in the actuator (Fig. 4).

The principle of operation of the laser sensor is as follows. A laser beam generated by the sensor is incident upon a reflective surface (the piece of silicon serves this purpose) on the diaphragm. The reflected beam returns through the same sensor opening, whereupon it passes through an optical system and is projected on photodiodes. As the target moves back and forth, the position of the reflected beam translates on the photodiode surface where this translation is correlated with the motion of the target through calibration. The sensor acquired data at 25 kHz . The calibration of the sensor was conducted as such: with the sensor attached to a movable automated stage and the diaphragm fixed in a particular location, the laser was moved in increments of $1 \mu\text{m}$ toward the diaphragm with the signal response measured at each location. This nonlinear displacement-response curve then served as the calibration curve.

To make measurements, the laser was positioned at the location that allowed for the largest sensitivity over the measurable range. The diaphragm was then operated where the resulting dynamic signal response from the laser was translated to a deflection through the calibration curve. To estimate the overall measurement accuracy of the laser, the uncertainties associated with stage position, sensor resolution, calibration, and experimental repeatability were taken into account. For a typical value the total combined uncertainty was estimated by the root sum square to be $\pm 1 \mu\text{m}$. The measurements of the dynamic response of the diaphragm result in the central deflection of the membrane (Δ), and the frequency of diaphragm oscillation (f).

4 Results and Discussion

In this section results of the dynamic response of the piezoelectric membrane are presented first, following which the external flow field is characterized.

A synthetic jet with a cavity-diaphragm setup is a coupled system consisting of an electromechanical domain in the form of the diaphragm, and a fluidic/acoustic domain in the form of the resonant cavity. The system may be thought to possess two fundamental frequencies; one associated with the resonant frequency of the diaphragm and the other with the Helmholtz frequency of the cavity. In order to determine (i) the approximate frequency at which to operate the actuator, and (ii) to check for the validity of the incompressible actuator model, the frequency response of the diaphragm was determined. With the driving voltage fixed at 3 V , the driving frequency was swept in intervals of 20 Hz over a range of $0\text{--}3000 \text{ Hz}$ with the laser sensor measuring the central dynamic response of the membrane. Figure 6 shows the resulting deflection

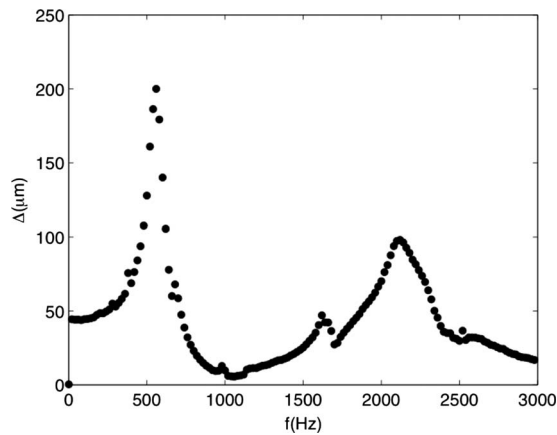


Fig. 6 The dynamic deflection response of the center of the piezoelectric diaphragm to the variation in driving frequency. Actuator 1, $V_d=30$ V.

frequency response of the diaphragm where three peaks are observed. The following expression presents a simple formula for the fundamental frequency of a clamped circular membrane [38]

$$f_d = 0.4705 \frac{p}{R^2} \sqrt{\frac{E}{\rho(1-\nu^2)}} \quad (10)$$

where p is the thickness, R is the radius, and E , ρ , and ν are the modulus of elasticity, density, and Poisson's ratio of the membrane, respectively. Using the above formula, the peaks at 560 Hz and 2120 Hz may be associated with the natural resonant frequency of the membrane in modes (0,1) and (0,2). Furthermore, an expression for the Helmholtz frequency of a cavity is [38]

$$f_h = \frac{c}{2\pi} \sqrt{\frac{A}{(H+0.85h)V}} \quad (11)$$

where c is the speed of sound, A is the area of the orifice, and V is the volume of the cavity. While it is recognized that the occurrence of a rectangular slot as opposed to a circular orifice complicates determining the Helmholtz frequency, using both (i) Eq. (11) along with a calculated effective diameter, and (ii) an expression for a Helmholtz frequency of a slot resonator [39], the Helmholtz frequency was calculated to be greater than 4000 Hz. The location of the small peak at 1620 Hz may be a result of the coupled nature of the diaphragm-cavity system and could not be correlated with the Helmholtz frequency from the simple analytical expressions. In spite of this, it is evident that the first mode of the membrane is less than the Helmholtz frequency, allowing for flow in the actuator to be considered incompressible [33]. This gives support to the actuator model considered in Sec. 2.2. From Fig. 6, 560 Hz was selected as the frequency to subsequently operate the actuator as it maximized both the membrane deflection and exit velocity.

Next, the effect of the driving voltage at a fixed frequency was studied. With the frequency fixed at 560 Hz, the driving voltage was swept over a range of 0–5 V in intervals of 0.5 V. The dynamic response is seen to increase with driving voltage (Fig. 7). The slight nonlinear response may be attributed to the dynamics of the actuator at the particular operating frequency. With actuator 2 similar trends in the frequency and amplitude response were observed as well. Now, the deflection results provide the centerline deflection of the membrane (Δ), which serves as an input to the actuator model described in Sec. 2.2. For example for actuator 1, the linear increase in displacement with voltage (Fig. 7) corresponds directly to a stroke ratio range of $0 < L/h < 14$ and Reynolds number range of $0 < Re_{V_o} < 260$. As seen from the frequency response curve (Fig. 6) the amplitude of vibration and frequency are tied together, and thus do not permit the study of the effect of frequency independently of amplitude over a wide range.

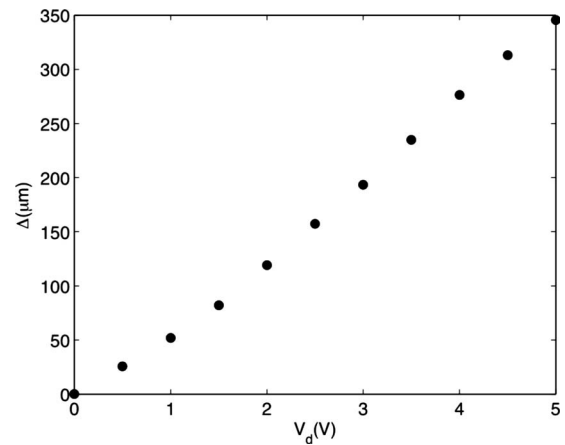


Fig. 7 The dynamic deflection response of the piezoelectric membrane at the center to the variation in driving voltage. Actuator 1, $f=560$ Hz.

With this constraint in mind experiments with varying driving parameters were conducted, where the test matrix for actuators 1 and 2 are summarized in Tables 1 and 2, respectively.

Measurements of the external flow field are now addressed and presented. They are the result of the average of three runs. First, the different regions that comprise the synthetic jet are identified. Figure 8 shows the axial progression of the streamwise time average velocity (U_c) along the centerline axis of the jet for actuator 2 for the four cases in Table 2. The flow field may be thought to be comprised of four regions. The first region, referred to as a developing region ($0 < x/h < 3$), is not captured in this experiment due to the limitations associated with the hot-wire mentioned in Sec. 3.1. However, it has been shown that in this region the velocity increases, reaches a maximum, and then starts to decrease [19]. The second region, referred to as a quasi-two-dimensional region ($3 < x/h < 25$), is where the velocity decays like a planar jet or as $x^{1/2}$. The third region, referred to as a transition region ($25 < x/h < 35$), is where the jet once again deviates from planar jet behavior, while further downstream the fourth region is where the jet starts to exhibit axisymmetric behavior. Results for actuator 2 are presented in Fig. 8 as three of the latter regions were clearly distinguishable. In actuator 1 the axisymmetric region was not observed as the jet decayed to such a point it could not be measured using the hot-wire, before the axisymmetric regime occurred.

Table 1 Test matrix for actuator 1 with $w/h=77$

Case no.	f (Hz)	V_d (V)	L/h	Re
1a	560	3	7.5	141
1b	560	3.5	9.3	173
1c	560	4	10.9	203
1d	560	4.5	12.3	230
1e	560	5	13.6	254

Table 2 Test matrix for actuator 2 with $w/h=45$

Case no.	f (Hz)	V_d (V)	L/h	Re
2a	560	1.5	2.5	137
2b	560	2	4.2	228
2c	560	2.5	5.1	275
2d	560	3	5.8	311

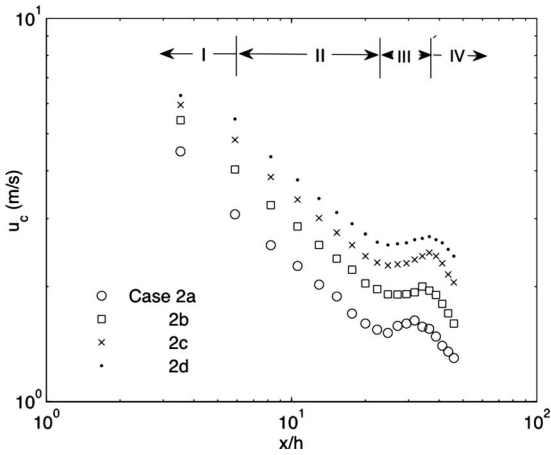


Fig. 8 Variation in the time average centerline velocity with axial distance, displaying the I: developing, II: quasi-two-dimensional, III: transition, and IV: axisymmetric regions (Actuator 2, see Table 2 for details of cases)

While the details of the developing region are not captured in this study, the region is known to be characterized by the periodic formation and advection of coherent vortical structures. As the stroke length increases it has been observed that both the extent of, and the peak velocity in this developing region increase [21]. This may be attributed to the increased slug length and momentum accompanying an increase in stroke ratio, and the resulting increased distance over which the initial development of the jet takes place. This being said, Fig. 8 clearly shows the velocity in a synthetic jet at an axial station increases with stroke ratio.

The quasi-two-dimensional region follows the developing region and extends to about $25 x/h$ from the orifice for all cases. In this region the central portion of jet may be approximated as a planar turbulent jet as the edge effects are not perceived here, as they continue to penetrate toward the center of the flow. It is this regime that the planar jet model applies to. With the centerline velocity decay expressed by Eq. (4), the variation in the decay constant K_u with an increase in displacement amplitude for both actuators is shown in Fig. 9. It is seen that in both cases that the velocity decay rate when plotted against the stroke ratio increase. However, the rate of increase is different suggesting that the actuator geometry plays a role in rectangular jet characteristics. The error associated with the decay rate is estimated to be 2%.

As seen from Fig. 6, due to the rather sharp deflection response it was not possible to study the effect of frequency over a large range on account of a lack of a measurable issuing jet beyond a

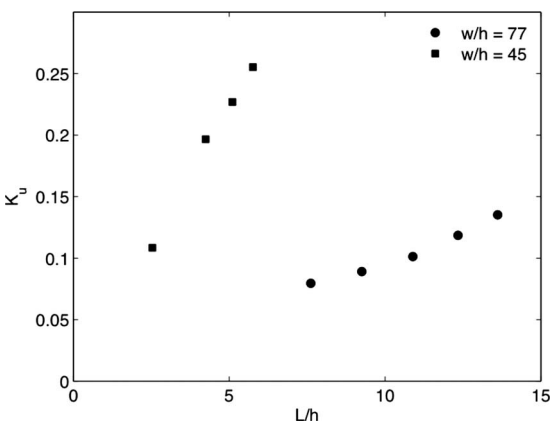


Fig. 9 Dependence of centerline decay rate on stroke ratio for both actuators

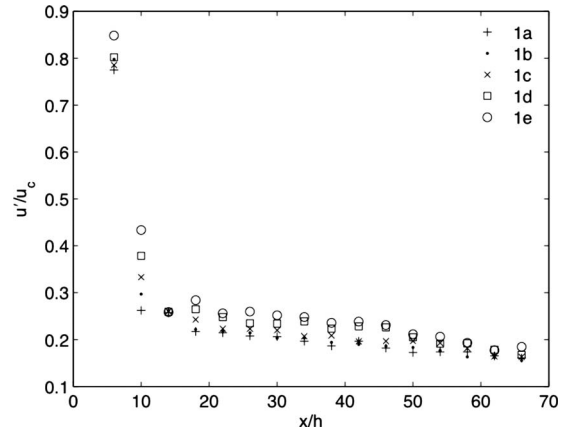


Fig. 10 Streamwise evolution of turbulence intensity at the centerline (Actuator 1, see Table 1 for details of cases)

certain limited window. However, in order to evaluate solely the effect of frequency, the driving voltage was fixed at 3 V while two frequencies ($f=480$ Hz and $f=620$ Hz) that yield approximately the same deflection ($105 \mu\text{m}$) and consequently stroke ratios were selected. It was seen that there was no significant difference in spreading rate and velocity decay rate for both cases. While the frequency range was limited, the results do support other workers data [18], suggesting that jet spreading and velocity decay are independent of Reynolds number, which is connected to the frequency via Eq. (9). The exact nature of the relationship between the velocity decay, spreading rate, and stroke ratio is however seen to be dependent on the geometry of the actuator.

The transition region is quite indicative of the influence of the finite slot width and is a result of the complex interaction of the periodic vortex structures emerging from the slot. The time average centerline velocity reached a local minimum then increases momentarily, and then starts to decay. This increase is thought to be due to the effect of the meeting and interaction of the off-center velocity peaks (Fig. 13) at the centerline. The jet starts to decay once again at a more rapid rate than in the quasiplanar regime, suggesting that the jet is transitioning to an axisymmetric jet, as is seen in continuous rectangular jets in the far field [40].

The axial variation in streamwise turbulent intensity is shown in Fig. 10. In the developed region large intensities are shown to be present. It should be noted that on account of the very high turbulent intensities in this region the time average velocities in the developing region should be interpreted qualitatively, as a single hot-wire introduces large errors either by overestimating the time average flow, or underestimating the rms velocity [41]. In this region the axial development of the turbulence intensity is thought to be the result of the manner in which (i) the initial turbulence at the orifice decays, and (ii) the coherent structures breakdown toward a turbulent flow. The increase in turbulence intensity with L/h may once again be attributed to the increase in the vigorous mixing that is brought about by the increase in both momentum and volume associated with the periodically formed vortical structures.

Figure 11 shows the transverse time average velocity profiles in the quasi-two-dimensional region at different streamwise stations. The streamwise velocity and lateral distance are normalized by the centerline velocity and streamwise distance from the velocity virtual origin, respectively. From Fig. 8 it is observed that as the jet moves downstream it slows down, and from Fig. 11 it may be deduced that the jet widens due to the entrainment of the surrounding fluid. The profiles collapse reasonably well in the central region, and appear to be self-similar and Gaussian in nature. Error bars are selectively shown in two locations, at $y-y_o/x=0.1$ and 0.5 for representative purposes. Toward the periphery of the jet

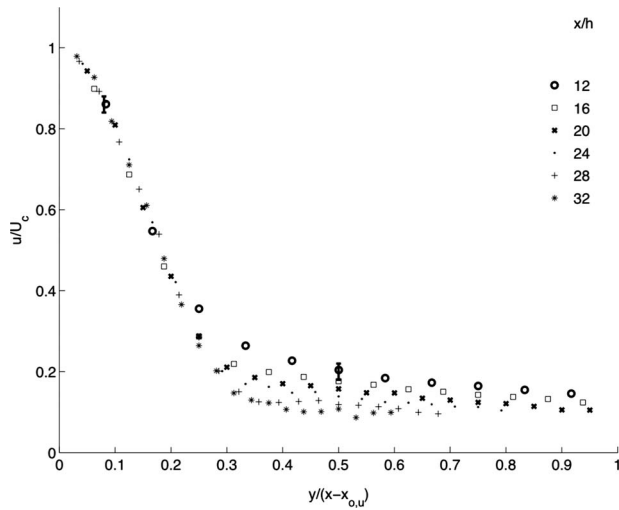


Fig. 11 Normalized time average streamwise velocity profile (Case 1a)

($y - y_0/x > 0.5$) the velocity is both low and contains a significant radial component. In this region the limitations of using a single normal hot-wire arises. As mentioned previously, the uncertainty due to this limitation was not quantified in this study.

Figure 12 shows the streamwise turbulent intensity profiles along the minor plane, with the turbulent fluctuation and lateral distance normalized by the centerline velocity and streamwise distance from the virtual origin, respectively. As the jet moves downstream the profile moves from a Gaussian shape to one that shows a distinct noncentral peak and the profiles appear to continue to develop. The turbulence intensity as with any shear flow tends to become self-similar further downstream in comparison to the time average flow, as the turbulence reacts slower to local conditions. Since the turbulence intensity profiles have not yet achieved self-similarity it would not be possible to say if the synthetic jet is less or more turbulent than an equivalent continuous jet.

The streamwise time average velocity profiles in the major plane are shown in Fig. 13. A distinct peak is noticed away from the center, the location of which moves toward the centerline line in the downstream direction and disappears far downstream (not seen in the graph). This saddle back profile has been observed both in synthetic [8] and continuous rectangular jets as well [42–44]. While reflective of the finite nature of the rectangular slot, several explanations have been offered to interpret the phenomena that include the interaction of streamwise [42] and cir-

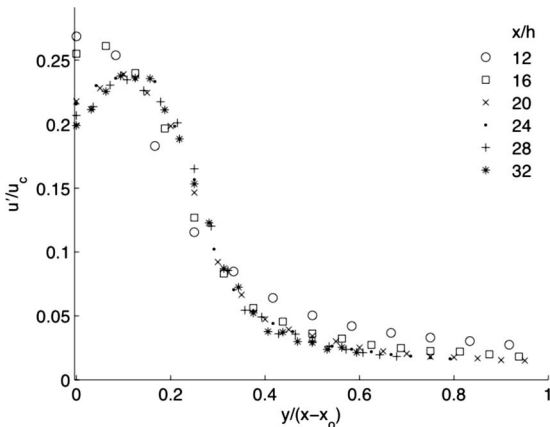


Fig. 12 Normalized fluctuating streamwise velocity profile (Case 1a)

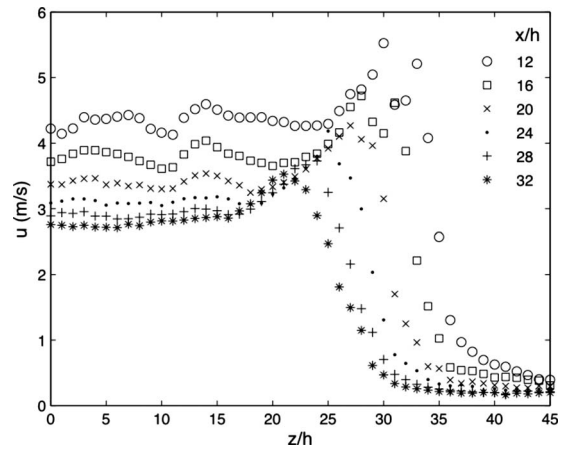


Fig. 13 Time average velocity profile along the major axis at different axial locations (Case 1a)

cumferential vortices [43] with the time average flow, resulting in a secondary flow that cause the peaks. It has also been suggested that the centrifugal forces developed result in a pressure distribution that cause fluid to move away from the center of the jet and toward the peaks [44]. In synthetic jets it has been observed that the edge induced counter-rotating vortex structures migrate inwards on account of their mutual attraction [8]. It is plausible that the time average flow on account of the vortex rotation may result in fluid moving toward the location of the observed peaks. The vortex pairs move inwards on account of mutual interaction, which is consistent with the movement of the peaks inwards. The central portion of the region however appears relatively flat suggesting that approximating the lateral velocity profile in the central region to be two-dimensional is feasible. The streamwise turbulent intensity profiles in the major plane (not shown) exhibit this saddle back profile as well, where the off-center peaks moved closer to the centerline as the flow moved downstream. The maximum streamwise turbulence intensity in the central major plane was observed to be higher than that in the central minor plane due to steep velocity gradients accompanying the saddle shape time average velocity profiles.

The axial variation in lateral width of the jet ($b_{1/2}$) within the quasi-two-dimensional region is shown in Fig. 14. Initially the jet width increases slowly, however beyond $x/h \approx 15$ the growth is more rapid and linear, further reinforcing the planar jet behavior.

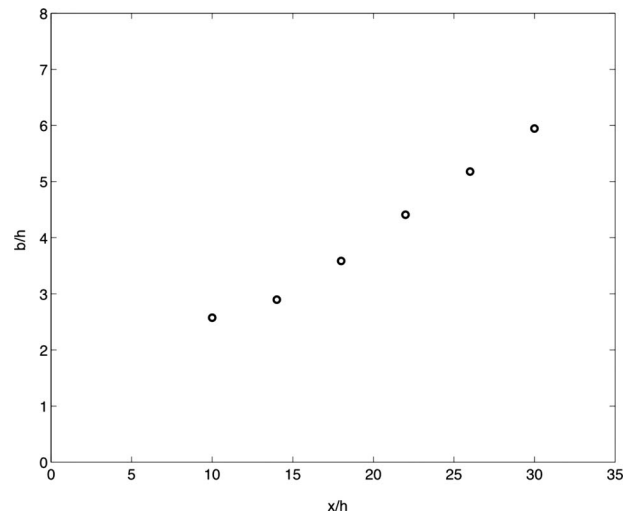


Fig. 14 Variation in jet half width with axial distance (Case 1a)

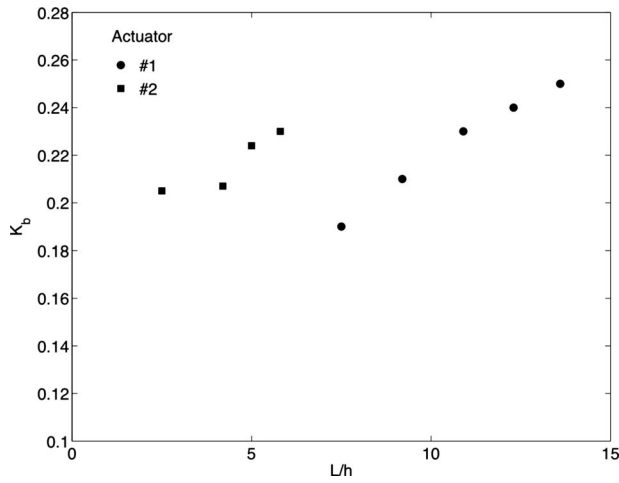


Fig. 15 Variation in spreading rate with increasing stroke ratio for both actuators

The lateral spreading rate for case 1a was calculated to be 0.19, which is greater than the spreading rate of a turbulent continuous jet of 0.11. Consequently for the synthetic jet $\sigma=4.6$, in comparison to 7.67 for a continuous jet. With the plane jet spreading rate expressed as Eq. (5), an increase in the driving voltage was observed to increase the lateral spreading rate (K_b) as shown in Fig. 15 for both actuators. As mentioned earlier the spreading rates show dependence on the geometry of the actuator. The error based on the uncertainty in velocity measurements, stage position, and curve fitting are estimated to be between 3% and 7%.

Figure 16 presents the variation in the eddy viscosity (Eq. (6)) with stroke ratio for the two actuators. The eddy viscosity of an equivalent continuous jet is also shown for comparison. Synthetic and continuous jets of the same orifice width (h) are considered equivalent in this investigation based on momentum flux, or otherwise if the steady bulk exit velocity of a continuous jet is equal to the time average velocity of a synthetic jet as calculated from $U_o = \sqrt{2fL}$. The eddy viscosity of the synthetic jet is seen to far exceed that of the equivalent continuous jet. The effect of employing a velocity scaling based on mass flux is to reduce the eddy viscosity as reported in Fig. 16 by a factor of $\sqrt{2}$. With the eddy

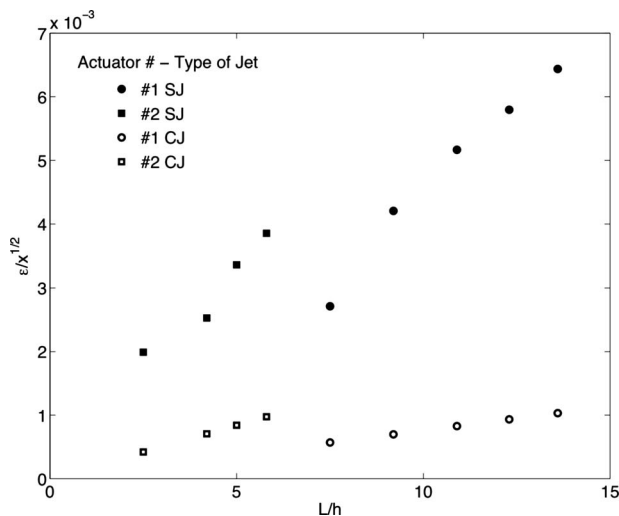


Fig. 16 Dependence of eddy viscosity (ϵ) on stroke ratio for the two synthetic jet actuators. The eddy viscosity of equivalent turbulent continuous jets are shown for comparison: CJ-continuous jet and SJ-synthetic jet.

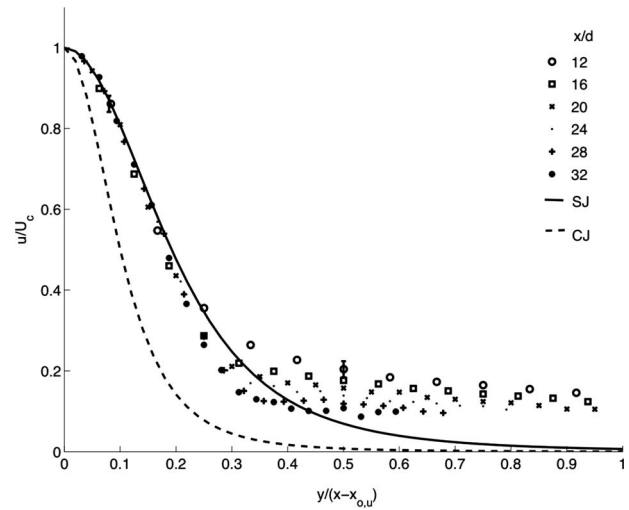


Fig. 17 Comparison of the analytical model and experimental data of a synthetic jet (Case 1a)

viscosity encompassing the capacity to transfer momentum to the surrounding fluid, it appears that the periodic nature of a synthetic jet greatly enhances the momentum transfer in comparison to continuous jets. The observed increase in the spreading rate, velocity decay rate, and eddy viscosity with stroke ratio may be explained as follows. It is known that the interactions of the large-scale coherent vortical structures in a jet are primarily responsible for mixing and spreading. An increase in excitation amplitude or otherwise stroke ratio results in an increase in the size of the slug (and subsequent vortical structure) issuing from the orifice. This slug additionally has an increased impulse and energy associated with it. This increased volume, impulse, and energy result in enhanced interactions further downstream, resulting in increased spreading and more rapid decay [2,19]. This higher eddy viscosity of the synthetic jet makes it appropriate for applications where changes in the surrounding fluid are desired as in fluid mixing or flow control.

Figure 17 compares the analytical time average velocity profiles of the jet obtained from Eq. (2) with the experimental data. A profile of an equivalent continuous turbulent jet with a spreading rate of 0.1 is presented for comparison. Error bars are selectively shown in two locations at $y-y_o/x=0.1$ and 0.5 for representative purposes. Other points in the bell part of the plot have error bars with similar magnitude. The enhanced mixing present in the synthetic jet in comparison to the continuous jet is clearly seen. The model approximates the data well toward the center of the jet thereby validating the eddy viscosity replacement hypothesis. However, progressing away from the center there is some deviation where the model underpredicts the flow. This discrepancy between the self-similar solution and the experimental data has also been observed in turbulent jets; see page 119 of Ref. [45]. This has been attributed to the constant eddy viscosity assumption in the self-similar solution. Here, we observe similar discrepancy for a synthetic jet. It is also plausible that toward the edges the flow is not predominantly in the streamwise direction, and thus the hot-wire measurement are less accurate [30,46]. Additional velocity components in the cross-stream or spanwise direction would result in the hot-wire measurements being higher than the true value which may explain why the model under predicts the velocity there [46].

5 Conclusions

The external flow field of a rectangular synthetic jet was studied using hot-wire anemometry. Four regions as distinguished by the centerline velocity were recognized. (i) An initial developing re-

gion where the coherent periodic vortical structures exist and interact, (ii) a quasi-two-dimensional region where the jet exhibits characteristics similar to a planar continuous jet, (iii) a transition region where the jet once again deviates from planar jet behavior on account of the spreading influence of the narrow edges, and (iv) an axisymmetric region where the jet starts to decay like a round jet. In the quasi-two-dimensional region the time average velocity profiles in the lateral direction exhibit self-similar behavior. The centerline velocity decay and jet width growth show trends similar to a continuous turbulent jet. This similitude leads to the hypothesis that the synthetic jet may be modeled as a continuous turbulent jet with the replacement of the eddy viscosity of a turbulent jet with that of a synthetic jet. The systematic modeling of the synthetic jet is carried out to show that similar to a continuous turbulent jet, the eddy viscosity of a synthetic jet can be obtained from the spreading and decay rates of the jet. The experiments on the flow field validate this hypothesis, further showing the eddy viscosity of the synthetic jet is larger than an equivalent continuous turbulent jet. This enhanced eddy viscosity is attributed to the additional mixing brought about initially by the introduction of the periodic vortical structures and their ensuing break down and transition to turbulence. Therefore by using the adjusted value of the eddy viscosity, the theoretical models of a continuous turbulent jet may still be used to model a synthetic jet. Within the small range tested, the velocity decay rate and spreading rate were insensitive to Reynolds number. However, both parameters increase with an increase in stroke ratio. The study shows a semi-analytical method in modeling synthetic jets that connects (i) the external flow field as characterized by the spreading rate (K_b) and velocity decay rate (K_d) to the actuator parameters ($L/h, Re_{U_o}$), and (ii) the actuator parameters to the input driving function (Δ, f).

While the above analysis and method provided useful tools for modeling the synthetic jet, there is still work that needs to be addressed. First an extensive parametric study is needed to assess the effects of the geometry and actuation parameters on the issuing synthetic jet. A thorough study characterizing the variable space may lend itself to a functional relationship between the spreading/decay rates to the geometric and operational parameters as represented below.

$$K_u, K_b = f\left(\frac{L}{h}, Re_{U_o}, \frac{h}{H}, \dots\right) \quad (12)$$

This study may then show that certain variables are not critical, thus reducing the number of variables resulting in some simplification. Second, at a fundamental level, the classic similarity analysis employed in this study assumes that the jet originates from a constant source of momentum. Even though the far field of a synthetic jet may be approximated by the results of the classic analysis, the constant momentum efflux is clearly not realized in a synthetic jet. Thus the next step in terms of analysis would be to seek a connection between an oscillatory transient point source of momentum and the ensuing steady flow that develops far from the source. This may further yield a clearer description of the evolution particular to a synthetic jet. Both these areas are topics of future work.

Acknowledgment

The authors thank Mr. Yunfei Wang for his initial contribution to the experiment, and the reviewers for their insightful comments that added clarity to the paper.

Nomenclature

K	= kinematic momentum flux per unit length (m^3/s)
L	= length of slug (m)
Re_{U_o}	= Reynolds number
T	= time period of oscillation (s)

f	= frequency of oscillation (Hz)
h	= width of orifice (m)
r	= radial coordinate on membrane
u	= time average streamwise velocity (m/s)
v	= time average transverse velocity (m/s)
w	= spanwise length of orifice (m)
x	= streamwise coordinate
y	= transverse coordinate
z	= spanwise coordinate
ε	= eddy viscosity (m^2/s)
η	= self-similar variable
ρ	= density of fluid (kg/m^3)
τ	= turbulent shear stress (Pa)
Δ	= centerline peak to peak deflection of membrane (m)
$b_{1/2}$	= jet half width (m)
K_b	= spreading rate
K_u	= scaled velocity decay constant
U_c	= centerline streamwise velocity (m/s)
U_o	= average actuator exit velocity (m/s)
V_d	= driving voltage (V)
$x_{o,u}$	= axial location of virtual origin based on velocity (m)
$x_{o,b}$	= axial location of virtual origin based on width (m)

References

- [1] Glezer, A., and Amitay, M., 2002, "Synthetic Jets," *Annu. Rev. Fluid Mech.*, **34**, pp. 503–529.
- [2] Utturkar, Y., Holman, R., Mittal, R., Carroll, R., Sheplak, B., and Cattafesta, L., 2003, "A Jet Formation Criterion for Synthetic Jet Actuators," 41st Aerospace Sciences Meeting and Exhibit, Reno, NV, AIAA Paper No. 2003-0636.
- [3] Holman, R., Utturkar, Y., Mittal, R., Smith, B., and Cattafesta, L., 2005, "Formation Criterion for Synthetic Jets," *AIAA J.*, **43**(10), pp. 2110–2116.
- [4] Amitay, M., Smith, B., and Glezer, A., 1998, "Aerodynamic Flow Control Using Synthetic Jet Technology," 36th Aerospace Sciences Meeting and Exhibit, Paper No. 98-0208.
- [5] Seifert, A., Eliahu, S., Greenblatt, D., and Wagnanski, I., 1998, "Use of Piezoelectric Actuators for Airfoil Separation Control," *AIAA J.*, **36**(8), pp. 1535–1537.
- [6] Rathnasingham, R., and Breuer, K., 2003, "Active Control of Turbulent Boundary Layers," *J. Fluid Mech.*, **495**, pp. 209–233.
- [7] Mahalingam, R., and Glezer, A., 2005, "Design and Thermal Characteristics of a Synthetic Jet Ejector Heat Sink," *ASME J. Electron. Packag.*, **127**(2), pp. 172–177.
- [8] Pavlova, A., and Amitay, M., 2006, "Electronic Cooling Using Synthetic Jet Impingement," *ASME J. Heat Transfer*, **128**(9), pp. 897–907.
- [9] Davis, S. A., and Glezer, A., 1999, "Mixing Control of Fuel Jets Using Synthetic Jet Technology," AIAA Paper No. 99-0447.
- [10] Parviz, B., Najafi, K., Muller, M., Bernal, L., and Washabaugh, P., 2005, "Electrostatically Driven Synthetic Microjet Arrays as a Propulsion Method for Micro Flight—Part I: Principles of Operation, Modelling, and Simulation," *Microsyst. Technol.*, **11**(11), pp. 1214–1222.
- [11] Finley, T., and Mohseni, K., 2004, "Micro Pulsatile Jets for Thrust Optimization," 2004 ASME International Mechanical Engineering Congress and RD&D Expo, Anaheim, CA, Paper No. IMECE 2004-62042.
- [12] Vargas, Y., Finley, T., Mohseni, K., and Hertzberg, J., 2006, "Flow Characterization of a Synthetic Jet," 44th AIAA Aerospace Sciences Meeting and Exhibit, Reno, NV, AIAA Paper No. 2006-1422.
- [13] Krishnan, G., and Mohseni, K., 2007, "On the Modeling of a Synthetic jet as a Spherical Jet," Fifth Joint ASME/JSME Fluids Engineering Conference, San Diego, CA, Paper No. FEDSM2007 2007-37306.
- [14] Mohseni, K., 2006, "Pulsatile Vortex Generators for Low-Speed Maneuvering of Small Underwater Vehicles," *Ocean Eng.*, **33**(16), pp. 2209–2223.
- [15] Krieg, M., and Mohseni, K., 2008, "Thrust Characterization of Pulsatile Vortex Ring Generators for Locomotion of Underwater Robots," *IEEE J. Ocean. Eng.*, **33**(2), pp. 123–132.
- [16] Mallinson, S., Hong, G., and Reizes, J., 1999, "Some Characteristics of Synthetic Jets," *Proceedings of the 30th AIAA Fluid Dynamics Conference*, Norfolk, VA, AIAA Paper No. 1999-3651.
- [17] Cater, J., and Soria, J., 2002, "The Evolution of Round Zero-Net-Mass-Flux Jets," *J. Fluid Mech.*, **472**, pp. 167–200.
- [18] Shuster, J., and Smith, D., 2007, "Experimental Study of the Formation and Scaling of a Round Synthetic Jet," *Phys. Fluids*, **19**(4), p. 045109.
- [19] Smith, B., and Glezer, A., 1998, "The Formation and Evolution of Synthetic Jets," *Phys. Fluids*, **10**(9), pp. 2281–2297.
- [20] Smith, B., and Swift, G., 2003, "A Comparison Between Synthetic Jets and Continuous Jets," *Exp. Fluids*, **34**(4), pp. 467–72.

- [21] Fugal, S. R., Smith, B. L., and Spall, R. E., 2005, "Displacement Amplitude Scaling of a Two-Dimensional Synthetic Jet," *Phys. Fluids*, **17**(4), p. 045103.
- [22] Gutmark, E., and Grinstein, F., 1999, "Flow Control With Noncircular Jets," *Annu. Rev. Fluid Mech.*, **31**, pp. 239–272.
- [23] Grinstein, F., 2001, "Vortex Dynamics and Entrainment in Rectangular Free Jets," *J. Fluid Mech.*, **437**, pp. 69–101.
- [24] Rizetta, D. P., Visbal, M. R., and Stanek, M. J., 1998, "Numerical Investigation of Synthetic Jet Flowfields," AIAA Paper No. 98-2910.
- [25] Menon, S., and Soo, J.-H., 2004, "Simulation of Vortex Dynamics in Three-Dimensional Synthetic and Free Jets Using the Large-Eddy Lattice Boltzmann Method," *J. Turbul.*, **5**, Art. No. 32.10.1088/1468-5248/5/1/032
- [26] Zhong, S., Garcillan, L., Pokusevski, Z., and Wood, N., 2004, "A PIV Study of Synthetic Jets With Different Orifice Shape and Orientation," AIAA Paper No. 2004-2213.
- [27] Amitay, M. and Cannelle, F., 2006, "Evolution of Finite Span Synthetic Jets," *Phys. Fluids*, **18**(5), p. 054101.
- [28] Ravi, B., 2006, "Numerical Study of Large Aspect-Ratio Synthetic Jets," AIAA Paper No. 2006-315.
- [29] Mittal, R., Rampunggoon, P., and Udaykumar, H. S., 2001, "Interaction of a Synthetic Jet With a Flat Plate Boundary Layer," AIAA Paper No. 2001-2773.
- [30] Kotapati, R. B., Mittal, R., and Cattafesta, L. N., III, 2007, "Numerical Study of a Transitional Synthetic Jet in Quiescent External Flow," *J. Fluid Mech.*, **581**, pp. 287–321.
- [31] Schlichting, H., 1933, "Laminare strahlausbreitung," *J. Appl. Math. Mech.*, **13**, pp. 260–263.
- [32] Schlichting, H., 1979, *Boundary-Layer Theory*, McGraw-Hill, New York.
- [33] Gallas, Q., Holman, R., Nishida, T., Carroll, B., Sheplak, M., and Cattafesta, L., 2003, "Lumped Element Modeling of Piezoelectric-Driven Synthetic Jet Actuators," *AIAA J.*, **41**(2), pp. 240–247.
- [34] Glezer, A., 1988, "The Formation of Vortex Rings," *Phys. Fluids*, **31**(12), pp. 3532–3542.
- [35] Timoshenko, S., 1999, *Theory of Plates and Shells*, McGraw-Hill, New York.
- [36] Smith, B., and Swift, G., 2001, "Synthetic Jets at Larger Reynolds Number and Comparison to Continuous Jets," 31st AIAA Fluid Dynamics Conference and Exhibit, Anaheim, CA, AIAA Paper No. 2001-3030.
- [37] Johnstone, A., Uddin, M., and Pollard, A., 2005, "Calibration of Hot-Wire Probes Using Non-Uniform Mean Velocity Profiles," *Exp. Fluids*, **39**(3), pp. 527–534.
- [38] Blevins, R. D., 1995, *Formulas for Natural Frequency and Mode Shape*, Krieger, Malabar, FL.
- [39] Everest, F., 2000, *The Master Handbook of Acoustics*, McGraw-Hill, New York.
- [40] Krothapalli, A., Baganoff, D., and Karamcheti, K., 1981, "On the Mixing of a Rectangular Jet," *J. Fluid Mech.*, **107**, pp. 201–220.
- [41] Tavoularis, S., 2005, *Measurement in Fluid Mechanics*, Cambridge University Press, Cambridge, UK.
- [42] Marsters, G. F., 1981, "Spanwise Velocity Distributions in Jets From Rectangular Slots," *AIAA J.*, **19**(2), pp. 148–152.
- [43] Van Der Hegge Zijnen, B., 1958, "Measurements of Velocity Distribution in Plane Turbulent Jet of Air," *Appl. Sci. Res., Sect. A*, **7**(4), pp. 256–276.
- [44] Quinn, W., Pollard, A., and Marsters, G., 1983, "On "Saddle-Backed" Velocity Distributions in Three-Dimensional Turbulent Free Jets," AIAA Paper No. 83-1677.
- [45] Pope, S., 2000, *Turbulent Flows*, Cambridge University Press, New York.
- [46] Rumsey, C., Gatski, T., Sellers, W., Vatsa, V., and Viken, S., 2006, "Summary of the 2004 Computational Fluid Dynamics Validation Workshop on Synthetic Jets," *AIAA J.*, **44**(2), pp. 194–207.